AUTOMATIC SEGMENTATION OF THE BLADDER USING DEFORMABLE MODELS

María Jimena Costa, Hervé Delingette, Nicholas Ayache

{Jimena.Costa, Herve.Delingette, Nicholas.Ayache}@sophia.inria.fr

ABSTRACT

We are interested in the fully automatic delineation of the bladder in CT images in the frame of dose calculation for conformational radiotherapy. To this end we fit a series of 3D deformable templates to the contours of anatomical structures. The novelty of our approach resides in the ability to automatically adapt to different kinds of bladder images (homogenous, non–homogenous, contrasted or non–contrasted). The adaptation of the algorithm to inhomogeneities within the bladder improves the accuracy of the segmentation. We validate our approach on a database of tomodensitometric (CT) images of the lower abdomen of male patients.

1 Introduction

An essential part of the conformal treatment planning procedure is the segmentation of target volumes and organs at risk in CT images. Bladder and rectum are considered as the organs at risk that should be protected against high dose of radiation during treatment of prostate cancer.

Because of the difficulty to accurately and reliably delineate structures in medical images, this task has traditionally been assigned to medical experts. However, manual editing is not only tedious but particularly prone to errors, as assessed by various intra or inter-operator variability studies [1].

Our aim is the development of an automatic method for the localization of lower abdomen structures, to reduce the time interval between imaging and treatment.

We approach the issue of boundary finding as a process of fitting a series of deformable templates to the apparent contours of anatomical structures. We choose simplex meshes to model the templates, owing to their fairly simple geometry, which eases the incorporation of deformation constraints. Given the high variability of soft tissues, a locally affine registration algorithm based on the more stable pelvic bone structures is first applied to place the images within the same frame of reference. An initial simplex mesh then undergoes both global and local deformations to fit the boundaries of a patient–specific approximation of the target organ. The segmentation is then refined by deforming the model on the tomodensitometric image itself. The result can later be interactively modified and/or corrected by the user. We apply our method to the segmentation of the bladder.

2 PREVIOUS WORK ON BLADDER SEGMENTATION

The segmentation of pelvic structures is a difficult task since it involves soft tissues that present a very large variability in shape, size [2] and intensity, the latter depending on the presence (partial or total) or absence of a contrast agent.

Semi–automatic or interactive approaches for bladder segmentation allow the pratician to have better control over the segmentation process [3, 4]. However, they remain time consuming and, especially for large databases, an automatic approach is desirable.

2.1 Non–rigid registration approaches

These methods have been tested for CT bladder segmentation (see [5] for a combined segmentation and registration approach). However, the considerable inter and intra–patient variation in soft tissue (slimmer and less slim patients, filling of the bladder at the moment of the CT scan, presence of contrast agent) may cause nearby structures to undergo ”unnatural” deformations necessary for the atlas to adapt to each patient’s specific bladder shape.

2.2 Mathematical morphology approaches

Mathematical morphology approaches are useful for bladder segmentation, for several reasons: the topology of the shape is known, the methods are easier to automate, and they can be quickly tuned and computed. However, they are quite dependent on the quality of the image. Variations of these approaches for bladder segmentation have been tested in [6] and [7] (region growing based algorithms) and in [8] (watershed based algorithm).

2.3 Shape deformation approaches

Shape deformation approaches include geometric [9, 10] and parametric [11] deformable models. They are quite flexible, since shape priors may be incorporated [9, 12, 2, 13, 3, 10], an atlas can serve as initialization [14], they can be made to follow fuzzy criteria [11], and they allow for more than one structure to evolve simultaneously (e.g. the prostate and bladder, as in [2]). However, they often require either training [13] or user interaction [9, 3].

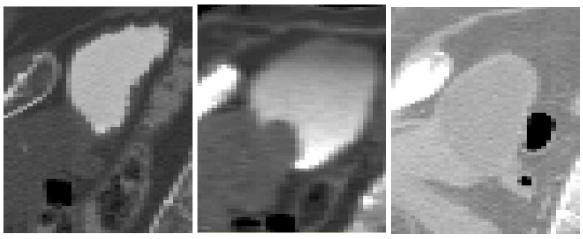

Fig. 1. Different types of bladders make the segmentation task challenging. From left to right, homogenous contrasted bladder, non–homogenous bladder and homogenous non–contrasted bladder (sagittal views).

3 METHOD

The bladders that appear in the CT images used in the previously cited approaches are homogenous and mainly non–contrasted. The interaction of an expert is often required either for initialization, or to choose patient–specific parameters. The novelty of our approach resides in the automatic initialization method (seed voxel detection) and the ability to adapt to different bladder images (homogenous intensity with high contrast, homogenous intensity with low contrast, or non–homogenous intensity with different contrast zones). A new histogram–based external force is also introduced.

3.1 Outline

Our approach is three–fold. It incorporates *non–rigid registration* based on surrounding bone structures to provide a reliable spatial initialization, *mathematical morphology* based operations to compute a good initialization of the underlying structure and *deformable models* to refine and smooth the segmentation while enforcing model constraints and forbidding segmentation "leakage" to neighboring soft tissue structures.

First, the bladder is located and classified as homogenous or non–homogenous, contrasted or non–contrasted (Figure 1). Then, the segmentation begins by computing an approximation of the structure through mathematical morphology operations. A simplex mesh is deformed to fit this approximation, and is later refined and smoothed using the bladder in the CT image itself. We are working on using these robust bladder segmentations for segmenting the prostate.

3.2 Preliminary processing

In order to put the CT images in a common reference frame, locally–affine registration [15] is performed on the pelvic bone structures (since they show lower variability than smooth tissues) and then interpolated to the other structures in the image. This allows us to perform the same cropping process on all the images to drastically reduce the computation time and also reduce or eliminate potential distractions for the algorithm (i.e., surrounding organs). We also determine whether the bladder shows the presence of a contrast agent or not, based on a threshold on the highest voxel intensity found among soft tissues. Later, the bladder will be labeled as homogenous (one zone of homogenous grey–level values) or non–homogenous (two main zones: a very contrasted "lower" zone and a less contrasted "upper" zone).

3.3 Initial structure approximation

A binary approximation of the structure is then computed. In order to obtain this approximation, we apply a modified version of seeded region–growing that incorporates mathematical morphology operations. A region growing algorithm with progressively laxer inclusion criteria and a closing operation is successively applied to the image, in order to obtain a series of rough partial segmentations of the bladder that eventually include it entirely. The morphological closing with a sufficiently large structuring element together with the evaluation of a stop criterion at each iteration allow us to avoid "leakage" of the region growing segmentation into surrounding structures (in particular, "thin" structures such as the seminal vesicles).

In the case of bladders showing the presence of a contrast agent, a region is progressively grown using a highly contrasted voxel located within a zone of low intensity variability as seed point. Since the location of the contrast agent is influenced by gravity, it tends to gather in the lower portion of the bladder. Therefore, we subsequently look for a potential "upper", non–contrasted region by looking for a seed point with similar characteristics to the first one (but different intensity range), near the upper part of the contrasted zone. If such a point is not found, the bladder is labeled as homogenous, and the segmentation of the contrasted zone is taken as an approximation of the whole bladder. On the other hand, if an upper region seed point is found, the bladder is classified as non–homogenous and a progressive region growing sequence is run for the upper part. The progression for different types of bladders is illustrated in Figure 2.

The process of progressive region growing provides us with the intensity based characteristics, such as mean and covariance matrix, that characterize each zone of the bladder.

3.4 Mesh deformation: binary stage

The binary approximation computed in the previous step serves to guide the preliminary stages of deformation (both global and local) of a simplex mesh.

A hierarchical approach is used: The initial mesh undergoes rigid and affine transformations that globally place the mesh as accurately as possible over the binary approximation of the bladder. After this step, the mesh begins to progressively undergo globally-constrained deformations [16], which allow it to adapt itself to smaller variations in the data.

The initial mesh deformation over a binary approximation of the target structure makes the whole procedure more robust in the presence of noisy data and outlier points in the original image. Further details on the deformation process can be found at [17].

3.5 Automatic division of the mesh into zones

In order to account for the high variability of the target structure, we adjust the deformable model to the type of bladder

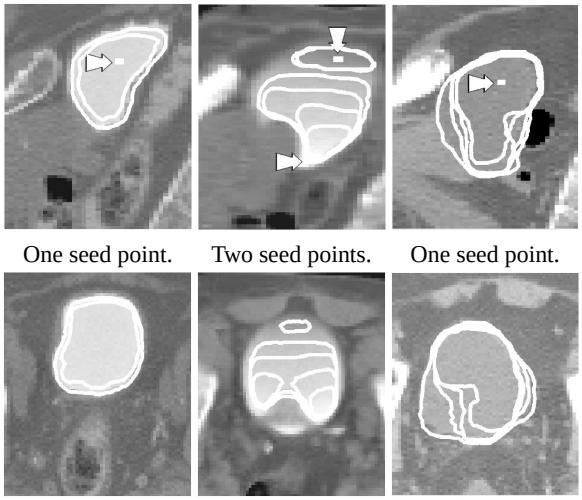

Fig. 2. Progression of modified region growing algorithms for different types of bladders (sagittal views). Seed points are indicated by arrows. The end result in each case will be the initial approximation that guides the first stages of the model deformation.

present in the image:

For *non–homogenous bladders*: The initial simplex mesh is divided into three zones. A Chamfer distance map is computed with respect to the segmented upper and lower zones. These distance maps are used to assign each vertex to upper, middle or lower zone. Each portion of the model will evolve under different forces, according to the characteristics of the target structure in the nearby region.

For *homogenous bladders*: Since the whole bladder has similar intensity properties, the mesh will deform itself globally under the same rules. Therefore, no zone division is needed.

3.6 Mesh deformation: gray–scale stage

Once the mesh properly delineates the binary approximation of the bladder, the segmentation is refined guided by the registered image itself and a histogram based force that we have devised to this end.

We propose an extended framework of deformable-model based image segmentation where the sought active contour or surface $\mathcal{S}(\mathbf{u}))$ results from the minimization of an energy. The surface $\mathcal{S}$ is pulled both towards $\mathcal{S}_{\mathrm{S}}$, a "smooth" surface that lies in the vicinity of $\mathcal{S}(\mathbf{u})$ (for regularization purposes) and $\mathcal{S}_{\mathrm{I}}$, an estimated target surface corresponding to the boundaries of an anatomical structure in an image.

We propose a *histogram–based* approach for estimating $\mathcal{S}_{\mathrm{I}}(\mathbf{u})$ given $\mathcal{S}(\mathbf{u})$ and $I[\mathbf{x}]$. In this method, the boundary points are assumed to be the ones for which the *inside voxels* have a high probability of belonging to the inside region while the *outside voxels* have a low probability of belonging to the inside region

Rather than basing the segmentation on an intensity range, we rely on the histogram of the interior of the current target structure, making no assumption on the intensities found in surrounding organs or on previous cases (training data).

If we assume that the normal $\mathbf{n}(\mathbf{u})$ at $\mathcal{S}(\mathbf{u})$ is oriented outwards, the boundary surface $\mathcal{S}_{\mathrm{I}}(\mathbf{u})$ can be computed at each iteration as $\mathcal{S}(\mathbf{u}) + s_\star\ \mathbf{n}$ with:

$$s_\star = \arg \min_{s\in[-L;L]} \sum_{v=-L}^{v=L} G_\sigma(|v-s|) * f(\mathcal{I}(\mathcal{S}(\mathbf{u})+v\ \mathbf{n}), \mu, \sigma, sgn(v-s))$$

where s is the position of each vertex of the final mesh we want to evaluate, v is the position of the voxels along the normal of the mesh at vertex s, and $f(i, \mu, \sigma, sgn)$ is a confidence estimation. This confidence is a piecewise constant function that serves to increase or decrease the energy term, depending on the values of two expressions: $|\frac{\mathcal{I}(\mathcal{S}(\mathbf{u})-\mu}{\sigma}| \leq 2$ and $sgn(v-s)$. For example, if the first term is false (i.e., the voxel's intensity is not compatible with the intensities found inside the structure) and the second term is true (i.e. the voxel is located inside the mesh), a positive penalization value is added to the energy term. Function G_σ defines a weight for the voxels that are taken into account at each iteration step; it may be a Gaussian p.d.f., a generalized rectangle function, or a combination of the two. The parameters are fully adjustable, to penalize more (or less) a non-homogeneity inside the structure or zone. If needed, at the end of the automatic segmentation process the results may be manually improved by an expert.

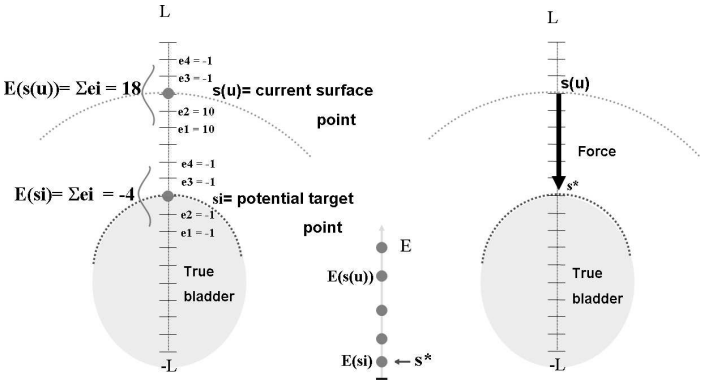

Fig. 3. Image voxels that are mistakenly included in the segmentation (inside the mesh) are heavily penalized (energy equals +10 in this example). Voxels that are correctly included or excluded in the segmentation have negative energy. The mesh will be pulled towards the potential surface that has minimal energy.

4 RESULTS AND PERSPECTIVES

The method has been tested in a database of CT images showing both homogenous and non–homogenous bladders. Figure 4 shows some quantitative measures of the results. The sensibility and the positive predictive value of the automatic segmentation with respect to the expert delineation have an average of 0.894 and 0.8695 respectively, with standard deviations of 0.0658 and 0.0721. The mean robust Hausdorff distance is of 3.34 mm with a standard deviation of 1.0855 mm. The segmentation process on a registered image takes less than a minute on a standard laptop computer. Some example results can be seen in Figure 5.

I	H	Sensib.	PPV	RHD
1	NH	0.94	0.73	2.7
2	H	0.96	0.80	3.0
3	H	0.87	0.81	3.7
4	NH	0.94	0.81	4.0
5	H	0.97	0.78	3.0
6	NH	0.93	0.81	3.0
7	NH	0.94	0.89	2.0
8	H	0.92	0.79	4.0
9	H	0.97	0.88	2.3
10	H	0.80	0.94	4.7

I	H	Sensib.	PPV	RHD
11	H	0.75	0.98	5.7
12	H	0.93	0.86	3.3
13	H	0.91	0.95	5.3
14	H	0.92	0.92	2.0
15	H	0.88	0.97	2.7
16	H	0.91	0.95	2.0
17	NH	0.84	0.93	3.7
18	NH	0.91	0.90	2.0
19	NH	0.83	0.86	4.0
20	H	0.76	0.83	3.7

Fig. 4. Sensibility, Positive Predictive Value and robust Hausdorff distance (95% quantile, all values in mm.) of the automatic segmentation with respect to the ground truth in homogenous (H) and non–homogenous (NH) bladder images.

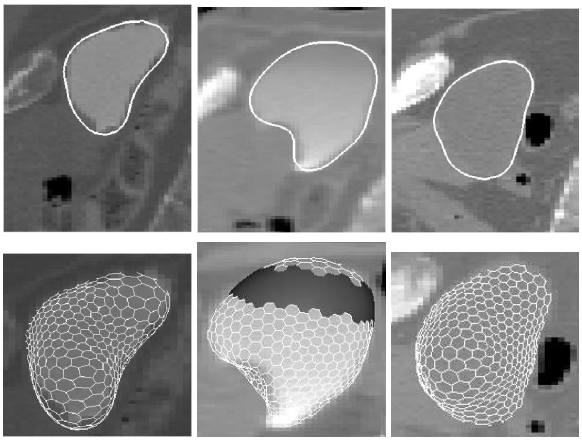

Fig. 5. Segmentation results (sagittal and 3D views). In the non–homogenous case (middle image), the 3 zones of the mesh (upper, middle and lower) can be seen.

The results are quite good, despite the variable quality of both the images and the expert segmentations. The modified region growing algorithm provides a good initialisation for both homogenous and non-homogenous bladders, while the mesh deformation steps improve or correct the final segmentation and apply a shape regularization as well.

The automatic segmentation is sometimes misled by a fuzzy bladder–prostate interface, which causes a "leakage" of the model into the latter and, consequently, an increased distance with respect to the expert delineation. We are able to partially avoid this by imposing strong regularization constraints on the model, but, as a side effect, the mesh is prevented from attaining high–curvature zones within the bladder. To address both problems and further improve the results, we are working on the simultaneous segmentation of the prostate and bladder with non–overlapping constraints on the models.

The work described in this article was performed in the framework of the European Integrated Project MAESTRO which is granted by the European Commission.

5 References

[1] D.C. Collier, S.S.C. Burnett, M. Amin, et al., " Assessment of consistency in contouring of normal-tissue anatomic structures. ," *Journal of Applied Clinical Medical Physics*, vol. 4, no. 1, 2003.

[2] M. Rousson, A. Khamene, M. Diallo, et al., "Constrained surface evolutions for prostate and bladder segmentation in ct images.," in *CVBIA*, Yanxi Liu, Tianzi Jiang, and Changshui Zhang, Eds. 2005, vol. 3765 of *Lecture Notes in Computer Science*, pp. 251–260, Springer.

[3] D. Freedman and T. Zhang, "Interactive graph cut based segmentation with shape priors," in *CVPR '05*, Washington, DC, USA, 2005, vol. 1, pp. 755–762, IEEE Computer Society.

[4] C.C. Lee and P.C. Chung, "Identifying abdominal organs using robust fuzzy inference model," in *IEEE International Conference on Networking, Sensing and Control*, Washington, DC, USA, 2004, vol. 2, pp. 1289–1294, IEEE Computer Society.

[5] G. Unal and G. Slabaugh, "Coupled pdes for non-rigid registration and segmentation," in *CVPR '05*, Washington, DC, USA, 2005, vol. 1, pp. 168–175, IEEE Computer Society.

[6] J. Camapum, A. Silva, A. Freitas, et al., "Segmentation of clinical structures from images of the human pelvic area," in *SIBGRAPI '04*, Washington, DC, USA, 2004, pp. 10–16, IEEE Computer Society.

[7] M. Mazonakis, J. Damilakis, H. Varveris, et al., "Image segmentation in treatment planning for prostate cancer using the region growing technique," *Br J Radiol*, vol. 74, no. 879, pp. 243–8, March 2001.

[8] G. Bueno, M. Fisher, K. Burnham, et al., "Automatic segmentation of clinical structures for rtp: Evaluation of a morphological approach.," in *Medical Image Understanding and Analysis*, 2001, pp. 73–76.

[9] F. Gibou, D. Levy, C. Cárdenas, et al., "Partial differential equations–based segmentation for radiotherapy treatment planning.," *Mathematical biosciences and engineering*, vol. 2, no. 2, pp. 209–226, 2005.

[10] R.E. Broadhurst, J. Stough, S.M. Pizer, et al., "Histogram statistics of local model-relative image regions.," in *DSSCV*, Ole Fogh Olsen, Luc Florack, and Arjan Kuijper, Eds. 2005, vol. 3753 of *Lecture Notes in Computer Science*, pp. 72–83, Springer.

[11] G. Bueno, A. Martínez-Albalá, and A. Adán, "Fuzzy-snake segmentation of anatomical structures applied to ct images.," in *ICIAR (2)*, Aurélio C. Campilho and Mohamed S. Kamel, Eds. 2004, vol. 3212 of *Lecture Notes in Computer Science*, pp. 33–42, Springer.

[12] S.D. Fenster, C.B.G. Kuo, and J.R. Kender, "Nonparametric training of snakes to find indistinct boundaries," in *MMBIA01*, 2001.

[13] D. Freedman, R.J. Radke, T. Zhang, et al., "Model-based multi-object segmentation via distribution matching," in *CVPRW '04*, Washington, DC, USA, 2004, vol. 1, p. 11, IEEE Computer Society.

[14] X. Ripoche, J. Atif, and A. Osorio, "A 3d discrete deformable model guided by mutual information for medical image segmentation," in *Proceedings of the Medical Imaging Conference 2004*. 2004, SPIE.

[15] O. Commowick, V. Arsigny, J. Costa, et al., "An efficient locally affine framework for the registration of anatomical structures," in *ISBI 2006*, Crystal Gateway Marriott, Arlington, Virginia, USA, April 2006, pp. 478–481.

[16] J. Montagnat and H. Delingette, "Globally constrained deformable models for 3d object reconstruction," *Signal Processing*, vol. 71, no. 2, pp. 173–186, December 1998.

[17] J. Costa, H. Delingette, J.-C. Diaz, et al., "Towards an automatic delineation of lower abdomen structures for conformational radiotherapy based on ct images," in *Proceedings of the 44èmes journées scientifiques de la Société Française de Physique Médicale (SFPM 2005)*, June 2005.